



Cite this: *Phys. Chem. Chem. Phys.*,  
2019, 21, 19163

## Structure and dynamic properties of stretched water in graphene nanochannels by molecular dynamics simulation: effects of stretching extent†

Mingbing Wu,<sup>a</sup> Wei Wei,<sup>a</sup> Xiaowei Liu,<sup>a</sup> Kang Liu<sup>\*b</sup> and Song Li  <sup>\*a</sup>

Water confined in nanochannels can be stretched with variation of the external pressure, leading to unusual properties compared with bulk water. In order to unravel the impacts of stretching extent on the structural and dynamic properties of water confined in hydrophobic graphene nanochannels with various channel widths ( $L = 1$  nm, 2 nm and 3 nm), molecular dynamics (MD) simulations were performed in this work. It was found that an ultrahigh negative pressure was present in the confined space with the increase of stretching extent before cavitation. The interfacial density peak and tetrahedral arrangement were reduced with the increasing hydrogen bond length, indicating the more disordered structural organization, especially in channels with small channel widths. On the other hand, the hydrogen bond lifetime was increased due to the prolonged stability of the hydrogen bond under stretching. The remarkably increased diffusion coefficients of confined water with the increasing stretching coefficient result from the faster diffusion of interfacial water along the channel surface regardless of channel width. At last, the oscillating tangential pressure profile inside the nanochannels demonstrated that the confined water under stretching consists of multiple layers exhibiting alternate positive and negative pressures, which is reduced with the increase of stretching coefficient, corresponding to the enhanced diffusion.

Received 16th July 2019,  
Accepted 6th August 2019

DOI: 10.1039/c9cp03981c

rsc.li/pccp

### 1. Introduction

Nanoconfined water, which plays a significant role in various fields including biology,<sup>1</sup> physics and chemistry,<sup>2</sup> and materials science,<sup>3</sup> has been attracting growing attention from both theorists and experimentalists in recent years. Both the structure and dynamic properties of water in nanoconfinement are remarkably different from bulk water.<sup>4,5</sup> The more ordered microstructure<sup>6</sup> and the accelerated transportation of water molecules under nanoconfinement<sup>7,8</sup> have been frequently reported by molecular dynamics (MD) simulations. The increased phase transition temperature of nanoconfined water in comparison with bulk water<sup>9,10</sup> has also been reported. In addition, the viscosity and the associated shear forces of confined water are increased by several orders of magnitude in contrast to bulk water.<sup>11</sup> The accelerated transportation of nanofluids<sup>12,13</sup> consisting of water confined in nanochannels

has won increasing research interest for decades.<sup>13,14</sup> Radha *et al.*<sup>15</sup> fabricated atomically flat 2D-capillaries experimentally and observed a significant enhancement in water flow (up to 1 meter per second) due to the high capillary pressures (approximately 1000 bar) and large slip lengths. Molecular simulation<sup>16</sup> has revealed that the flux of water within hydrophobic graphene is three to four orders of magnitude higher than that confined within hydrophilic hBN (hexagonal boron nitride) and MoS<sub>2</sub> of identical pore width, suggesting that the dynamic properties of nanoconfined water depend strongly on the channel surface properties.

Regardless of the enormous number of studies on confined water, the impacts of stretching or negative pressure have not been taken into account. It is known that the cohesion of liquid water can sustain an external mechanical stretching, resulting in an internal ultrahigh negative pressure,<sup>17</sup> *i.e.*, the water molecules are subjected to large hydrostatic tension. This is a common state for water in nature. For example, in the process of transpiration of plants,<sup>18,19</sup> the sap inside xylem is under stretching (*i.e.*, the absolute pressure of stretched water is negative) until cavitation breaks the continuity of water and hence water is supplied to transpiring leaves. Liquid water under tension in a metastable state can be utilized to drive fluid water in microchannels, which is the key for heat and

<sup>a</sup> State Key Laboratory of Coal Combustion, School of Energy and Power Engineering, Huazhong University of Science and Technology, Wuhan 430074, Hubei, China. E-mail: songli@hust.edu.cn

<sup>b</sup> MOE Key Laboratory of Hydrodynamic Transients, School of Power and Mechanical Engineering, Wuhan University, Wuhan, Hubei 430072, P. R. China. E-mail: kang.liu@whu.edu.cn

† Electronic supplementary information (ESI) available. See DOI: 10.1039/c9cp03981c

mass transfer in microfluidics.<sup>20</sup> The maximum pressure of stretched bulk water is predicted to be approximately  $-200$  MPa by MD simulations.<sup>21</sup> However, the pressure profile of stretched water in nanoconfinement has not been explored, which is critical for assessing the transportation performance of water in nanochannels.

It should also be noted that evaporation plays an equivalent role to stretching in creating negative pressures of water in confinement, and it is frequently employed for heat dissipation. Nazari *et al.*<sup>22</sup> have achieved unprecedented evaporative heat fluxes in nanochannels by utilizing the negative liquid pressure for thermal management of photonic and electronic devices. Excessive stretching or evaporation will result in cavitation, in which the negative pressure exceeds the critical points that confined water can sustain. Duan *et al.*<sup>23</sup> have directly observed evaporation-induced cavitation and accelerated water transport in nanofluidic channels driven by the negative pressure of up to  $-7$  MPa. Overall, nanoconfined water in negative pressure is common under stretching or evaporation in many processes. However, little effort has been made to investigate the impacts of channel width on the negative pressures presented by confined water. From another perspective, exploring the microstructure and dynamic properties of the stretched water molecules in nanochannels can facilitate our understanding towards the physiochemical properties of confined water from the view of negative pressure. Therefore, this work investigated the pressure profile, structure and dynamic properties of stretched water confined in graphene nanochannels by MD simulations.

## 2. Methodology

In this work, we considered  $N$  water molecules enclosed between two parallel graphene sheets. The TIP4P<sup>24</sup> water model with four interaction sites, including an additional massless M site located coplanar with the oxygen (O) and hydrogen (H) sites on the bisector of the H-O-H bond angle, was used for molecular simulations. Meanwhile, the carbon atoms of graphene sheets were modelled as neutral particles interacting with the oxygen atoms through the LJ parameters of  $\sigma = 3.4$  Å and  $\epsilon = 0.23227$  kJ mol<sup>-1</sup> taken from the Universal Force Field (UFF),<sup>25</sup> whose accuracy has been validated in our previous

study.<sup>26</sup> The LJ parameters of different atom pairs were calculated using the Lorentz–Berthelot combining rule (*i.e.*,  $\sigma_{ij} = 1/2(\sigma_i + \sigma_j)$  and  $\epsilon_{ij} = \sqrt{\epsilon_i \times \epsilon_j}$ ). The graphene channels with a width of  $L$  ranging from 1 to 3 nm are shown in Fig. 1. The dimensions of a graphene sheet containing 384 carbon atoms were 2.95 nm  $\times$  3.40 nm. The  $z$  dimension perpendicular to the graphene sheet varies for each system, namely  $L = 1$  nm, 2 nm and 3 nm.

The initial number of water molecules  $N$  in various nanochannels was determined by grand canonical Monte Carlo (GCMC) simulations in RASPA,<sup>27</sup> from which 224, 550 and 885 water molecules in graphene nanochannels of  $L = 1$ , 2 and 3 nm, respectively, were obtained. In order to generate different stretching extents of water in nanochannels, a number of water molecules were removed randomly from the channels, and then the system was equilibrated under the *NVT* ensemble by MD simulations for 2 ns, followed by a 5 ns production run. Thus, in total, 18 independent MD simulations for each nanochannel were carried out to compute the pressures at varying stretching extents. In order to quantify the stretching extent, stretching coefficient ( $c_N$ ) defined as the ratio of eventual number of water molecules to the initial number of water molecules in the channel in eqn (1) was adopted.

$$c_N = \frac{\Delta N}{N} \quad (1)$$

where  $N$  represents the initial number of water molecules in graphene channels, and  $\Delta N$  means the number of water molecules that were removed from the initial system. Therefore, each system containing a specific number of water molecules corresponds to a stretching coefficient or stretching extent. Some representative systems along with their corresponding number of water molecules of all graphene channels are shown in Table S1 (ESI†).

All MD simulations were performed in the *NVT* ensemble using the Gromacs package.<sup>28</sup> The constant target temperature of 300 K was applied and maintained by the Nose–Hoover with a time constant of 0.5 ps. The electrostatic interactions were computed directly by the Coulomb law up to 1.28 nm between the interaction sites, beyond which the PME<sup>29</sup> method was implemented. The time step of 1.0 fs was used to integrate the equation of motion. For each system, a total of 7 ns including 2 ns for equilibration and 5 ns for analysis was applied for MD

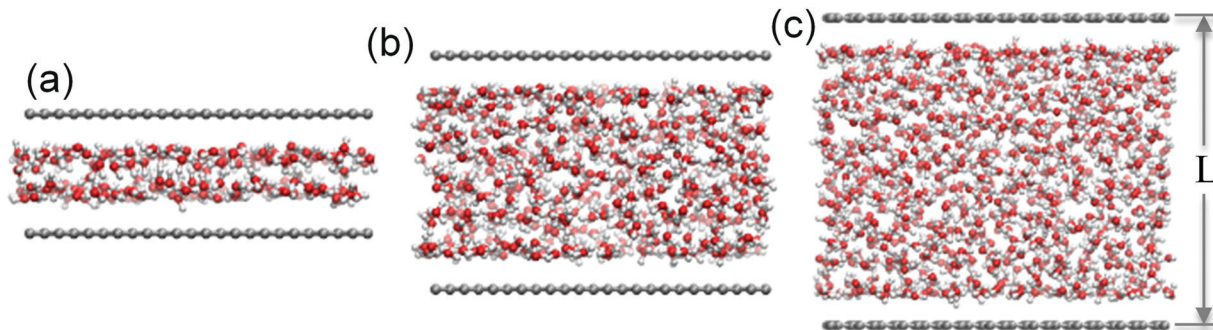


Fig. 1 A schematic diagram of water molecules confined within two parallel graphene sheets with a distance of (a)  $L = 1$  nm, (b)  $L = 2$  nm and (c)  $L = 3$  nm. Carbon, oxygen and hydrogen atoms are represented by spheres in grey, red and white, respectively.

simulations. Periodic boundary conditions (PBCs) were applied to all directions.

The corresponding pressure  $\mathbf{P}$  at each stretching extent is computed<sup>30</sup> as:

$$\mathbf{P} = \mathbf{P}_{\text{kin}} + \mathbf{P}_{\text{conf}} = - \begin{bmatrix} \sigma_{xx} & \sigma_{xy} & \sigma_{xz} \\ \sigma_{yx} & \sigma_{yy} & \sigma_{yz} \\ \sigma_{zx} & \sigma_{zy} & \sigma_{zz} \end{bmatrix} = \begin{bmatrix} P_T & 0 & 0 \\ 0 & P_T & 0 \\ 0 & 0 & P_N \end{bmatrix} \quad (2)$$

where  $\mathbf{P}$  is a second-order tensor for an inhomogeneous fluid, which includes a kinetic contribution ( $\mathbf{P}_{\text{kin}}$ ) from convective momentum transport of molecules and a configurational contribution ( $\mathbf{P}_{\text{conf}}$ ) due to interactions among molecules. The axial symmetry in the  $z$  dimension (normal to the pore walls) and translational symmetry in the  $xy$ -plane indicate that all off-diagonal components are zero, and there are only two independent, non-zero components: the tangential pressure (parallel to the wall)  $P_{xx} = P_{yy} = P_T = (P_{xx} + P_{yy})/2$  ( $P_{xx} = -\sigma_{xx}$ ,  $P_{yy} = -\sigma_{yy}$ ), and the pressure normal to the wall  $P_{zz} = P_N$  ( $P_{zz} = -\sigma_{zz}$ ). The virial stress is calculated<sup>31</sup> as

$$\sigma = \frac{2}{V} (\Xi - E_{\text{kin}}) \quad (3)$$

where  $V$  is the volume of the computational box. The kinetic energy and virial stress of the  $N$ -particle system can be calculated, respectively:

$$E_{\text{kin}} = \frac{1}{2} \sum_i^N m_i \mathbf{v}_i \otimes \mathbf{v}_i \quad (4)$$

$$\Xi = -\frac{1}{2} \sum_{\substack{i,j \\ i \neq j}} (r_i - r_j) \otimes F_{ij} \quad (5)$$

where  $m_i$  is the atomic mass associated with O and H sites only,  $r_i$  is the position vector and  $\mathbf{v}_i$  is the velocity vector.  $F_{ij}$  is the force vector between two interaction sites (O, H or M). Note that the ultimate pressure is computed as the ensemble average of each system.

The intermittent autocorrelation function (ACF),  $C(t)$ ,<sup>32</sup> was calculated according to eqn (6).

$$C(t) = \frac{\langle h(0)h(t) \rangle}{\langle h \rangle} \quad (6)$$

where  $h(t) = 1$  indicates that a specific water pair is hydrogen bonded at time  $t$  and 0 indicates otherwise (it may become 1 again later if the two water molecules reform the hydrogen bond).  $C(t)$  does not depend on the continuous presence of the hydrogen bond. The relaxation time  $\tau_{\text{rlx}}$  of  $C(\tau_{\text{rlx}}) = e^{-1}$  was calculated to measure the structural relaxation of the hydrogen bond.<sup>33</sup>

Self-diffusion coefficient ( $D$ ) is calculated from the mean square displacement (MSD) through the Einstein relation as follows:

$$D = \lim_{t \rightarrow \infty} \frac{1}{4Nt} \left\langle \sum_{i=1}^N [r_i(t) - r_i(0)]^2 \right\rangle \quad (7)$$

where  $r_i(0)$  and  $r_i(t)$  are the positions of the center of mass of the molecules at time 0 and  $t$ , respectively.  $D$  is the self-diffusion coefficient,  $N$  is the total number of molecules, and  $\langle \rangle$  means an ensemble average. Here, each ultimate value  $D$  is determined by averaging five independent simulations of 1 ns.

### 3. Results and discussion

The tangential pressure ( $P_T$ ) and normal pressure ( $P_N$ ) profiles of water confined in graphene channels of different widths with the increase of stretching coefficient are shown in Fig. 2a and b, respectively. Both tangential pressure ( $P_T$ ) and normal pressure ( $P_N$ ) were negative, indicating the high hydrostatic tension of liquid water under stretching, which also increased with the increase of stretching coefficient. The initial increase in pressure can be ascribed to the large tension required to sustain external strain until the critical cavitation pressure (*i.e.*, the maximum negative pressure), suggesting the increase in hydrostatic tension of water is associated with the onset of cavitation in water.<sup>21</sup> Further stretching causes the occurrence of cavitation, leading to a significant reduction in pressure. The corresponding  $\varepsilon_{N_{\text{max}}}$  for  $L = 1, 2$  and  $3$  nm was 0.20, 0.18 and 0.15, respectively, indicating that the water in the smaller

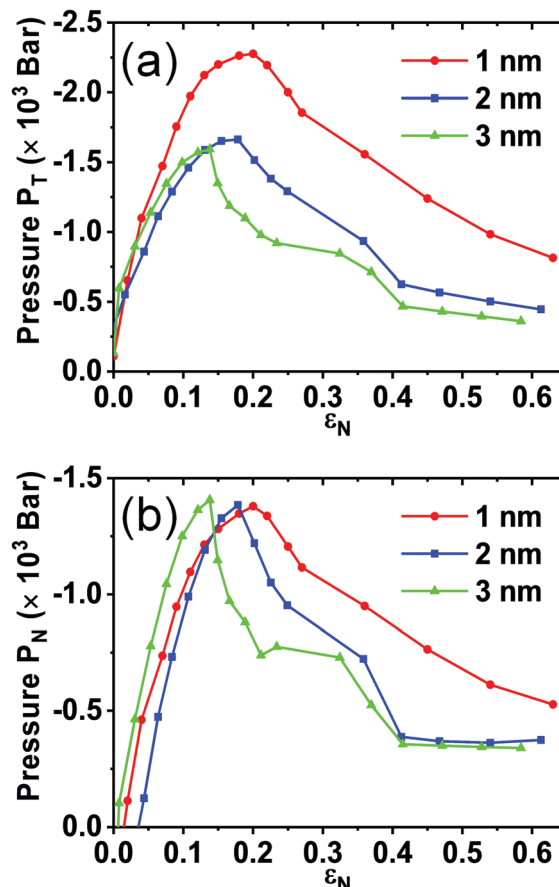


Fig. 2 (a) Tangential pressure ( $P_T$ ) and (b) the pressure normal to the wall ( $P_N$ ) of confined water inside various graphene channels of  $L = 1, 2$  and  $3$  nm as a function of stretching coefficient.

nanochannel can sustain a higher stretching extent. Additionally, the maximum negative tangential pressure ( $P_T$ ) of water in narrow channels ( $L = 1 \text{ nm}$ ) is higher (~2000 bar) than those in wide channels, implying the faster transport of water in smaller channels. Cavitation occurs at  $\varepsilon_{N_{\max}}$  and cavities grow with the stretching coefficient, consistent with previous observations in bulk water by MD simulation.<sup>21,34</sup>

In this work, we mainly focused on the microstructure and dynamic properties of confined water at varying stretching coefficients prior to cavitation ( $\varepsilon_N = \varepsilon_{N_{\max}}$ ). We firstly analysed the density distribution profiles of water along the direction perpendicular to the graphene surface computed according to the center of mass of water molecules, as shown in Fig. 3. The density distribution profiles of water confined in graphene nanochannels with varying widths ( $L = 1, 2, \text{ and } 3 \text{ nm}$ ) and stretching coefficients (*i.e.*,  $\varepsilon_N = 0, \varepsilon_N = \varepsilon_{N_{\max}}$  and  $0 < \varepsilon_N < \varepsilon_{N_{\max}}$ ) were compared. Apparently, all density profiles oscillate from the graphene interface to the intermediate region, which is a common phenomenon observed at solid–liquid interfaces.<sup>35–37</sup> In particular, there is an interspace of ~0.25 nm between graphene and water, beyond which the first peak extending up to 0.5 nm appears. Comparing profiles in Fig. 3a–c, the locations of the interspace and the first peak are independent of the nanochannel width, similar to many reports.<sup>35,38–40</sup> Only two oscillating density peaks were observed for  $L = 1 \text{ nm}$  (Fig. 3a), implying two-layer structures of confined water molecules.<sup>35,41</sup> For  $L = 2 \text{ nm}$  and  $L = 3 \text{ nm}$ , a bulk-like region at the central channel was formed (Fig. 3b and c), indicating that the effect of the surface perturbation is highly localized and amplified under extreme confinement (*i.e.*,  $L = 1 \text{ nm}$ ). During the process of stretching, the density peaks are reduced with the increase of stretching coefficient, and the density peak locations slightly shifted towards the central region regardless of channel widths owing to the varying orientation of water molecules in this region, which will be discussed in detail later.

To further investigate the effects of stretching coefficients on the structural properties of confined water, we calculated the tetrahedral order parameter ( $q$ )<sup>42</sup> that is frequently used to evaluate the structure order of water and orientation distribution probability profiles (Fig. 4). Tetrahedral order parameter  $q$

is a parameter describing the order of tetrahedral structure of water described as:

$$q = 1 - \frac{3}{8} \sum_{j=1}^3 \sum_{k=j+1}^4 \left( \cos \psi_{jk} + \frac{1}{3} \right)^2 \quad (8)$$

where  $\psi_{jk}$  represents the angle formed by one oxygen atom of one molecule and the other two oxygen atoms of the adjacent molecules.  $q$  varies from 0 to 1.  $q = 1$  represents the perfect tetrahedral network and  $q < 1$  represents the configuration deviating from the ideal tetrahedral structures.<sup>42,43</sup> Fig. 4a–c demonstrate that confined water exhibits a lower probability of tetrahedral structure compared to bulk water,<sup>43</sup> which may result from the aggregation of water molecules at the graphene surface. With the increase of channel width, the tetrahedral order parameter probability profiles tend to approximate to that of bulk water due to the enlarged bulk-like region of the central channels. With the increase of stretching coefficient, the profile of confined water shifted towards lower  $q$ , indicating that the higher the  $\varepsilon_N$ , the more disordered the confined water. This could be attributed to the growing intermolecular void space during stretching, characterized by void fraction<sup>44</sup> ( $V_F$ ), as shown in Table 1, which may inevitably destroy the formation of the tetrahedral structure of water molecules, leading to a shift toward low  $q$ . The void fraction is the ratio of the volume of intermolecular space that is accessible to the virtual probe sphere of 0.28 nm in radius to the volume of the channels, which was calculated by the Construct Surface Mesh Modifier of OVITO.<sup>45</sup> The radius of the probe sphere is determined according to the location of the first peak in the O–O radial distribution function of water.<sup>44</sup>

Additionally, the orientation distribution probability profile of confined water within the interfacial region (~0.5 nm) is shown in the inset of Fig. 4d. The dipoles of water molecules prefer to be perpendicular to the graphene surface, whereas the water plane defined as the vector of the two H atoms and the normal direction of the graphene surface prefers to be parallel to the graphene surface, as shown in Fig. S1 (ESI†), which may facilitate the formation of hydrogen bonds of water, similar to previous studies.<sup>40,46</sup> The increased channel widths will reduce the orientation tendency. Under the process of stretching,

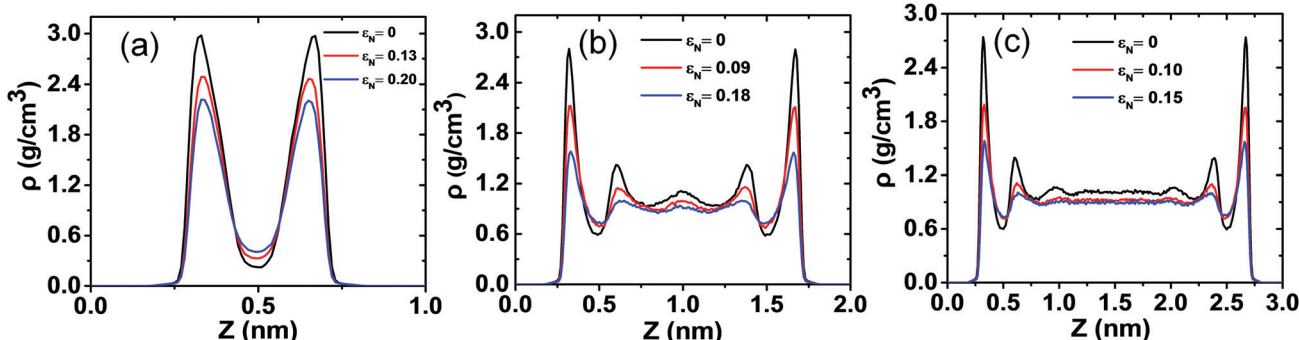


**Fig. 3** The density distribution profiles of confined water under different stretching coefficients along the direction perpendicular to the graphene surface at 300 K for (a)  $L = 1 \text{ nm}$ , (b)  $L = 2 \text{ nm}$  and (c)  $L = 3 \text{ nm}$ . Black and blue lines represent the density distribution profiles of confined water at  $\varepsilon_N = 0$  and  $\varepsilon_N = \varepsilon_{N_{\max}}$ , respectively. Red line represents the intermediate  $\varepsilon_N$ .

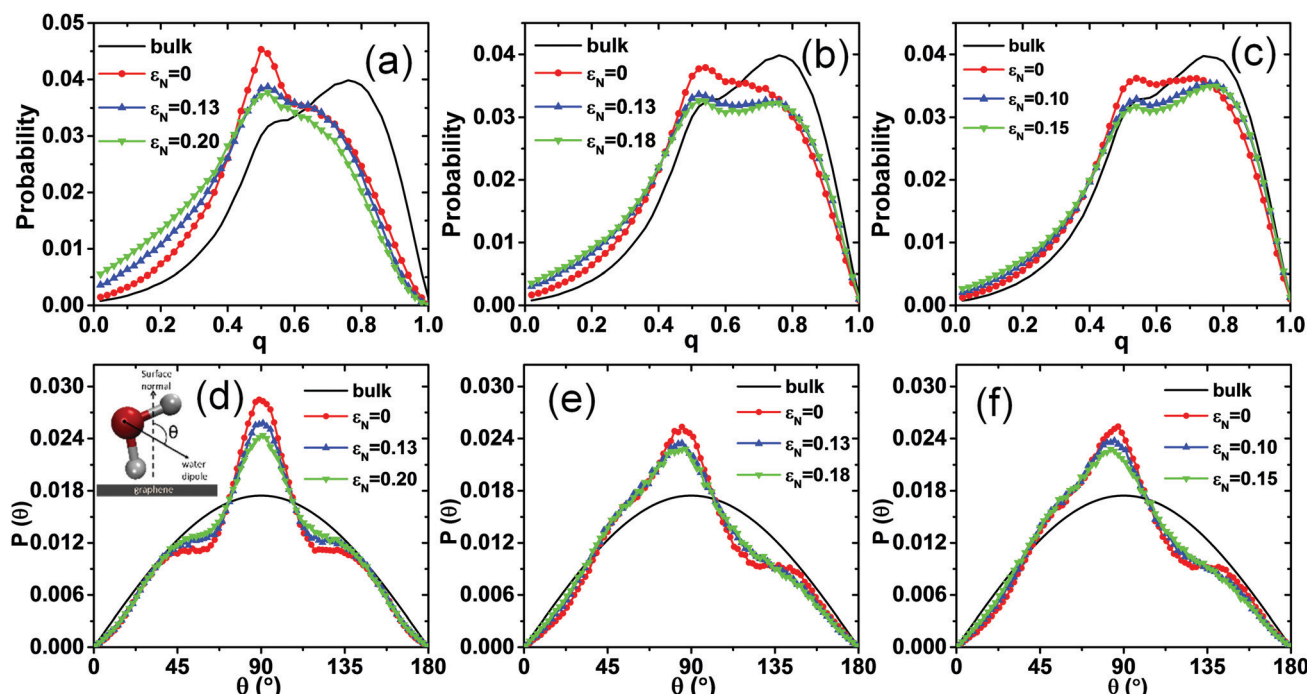


**Fig. 4** The tetrahedral order parameter ( $q$ ) and orientation distribution probability profiles of stretched water confined within various graphene channels at 300 K, respectively. The left, middle and right panels represent cases of (a and d)  $L = 1$  nm, (b and e)  $L = 2$  nm and (c and f)  $L = 3$  nm, respectively. Black solid lines represent the results of bulk water. The inset of (d) describes the angle formed between the water dipole and the normal vector of graphene surface.

**Table 1** The varying void fractions of stretched water inside graphene channels with different channel width

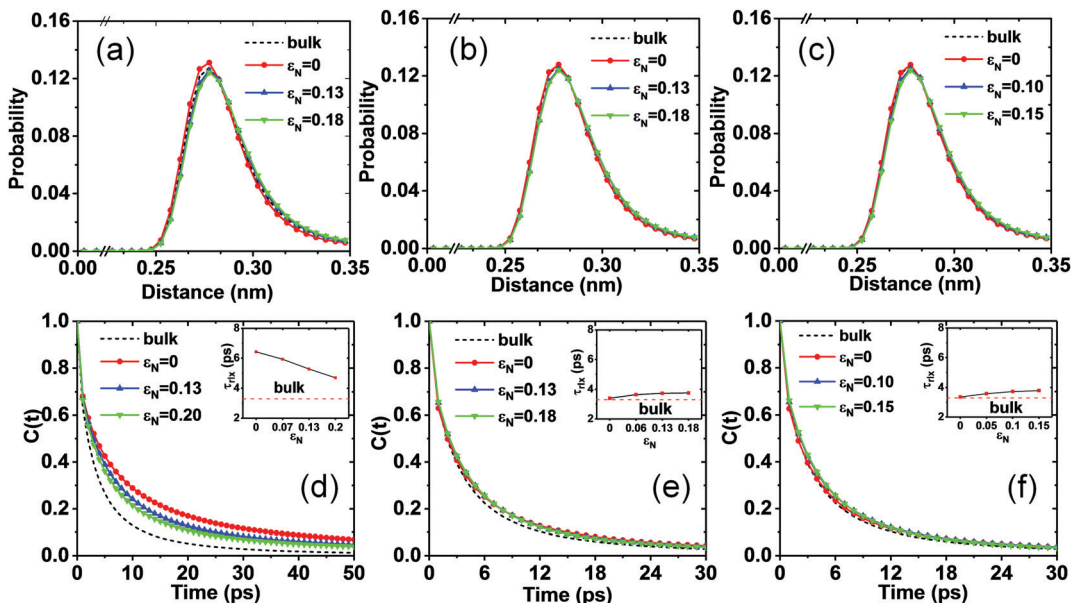
$L = 1$ nm		$L = 2$ nm		$L = 3$ nm	
$\varepsilon_N$	$V_f$ (%)	$\varepsilon_N$	$V_f$ (%)	$\varepsilon_N$	$V_f$ (%)
0	0.32	0	1.07	0	2.93
0.07	2.24	0.06	6.76	0.05	6.26
0.13	6.29	0.13	13.69	0.1	10.87
0.2	12.75	0.18	20.48	0.15	18.24

however, the planes of water exhibit less and less preference to be parallel to the graphene surface, because some water molecules slightly tilt toward the central region, in agreement with the peak of the water density profiles of Fig. 3.

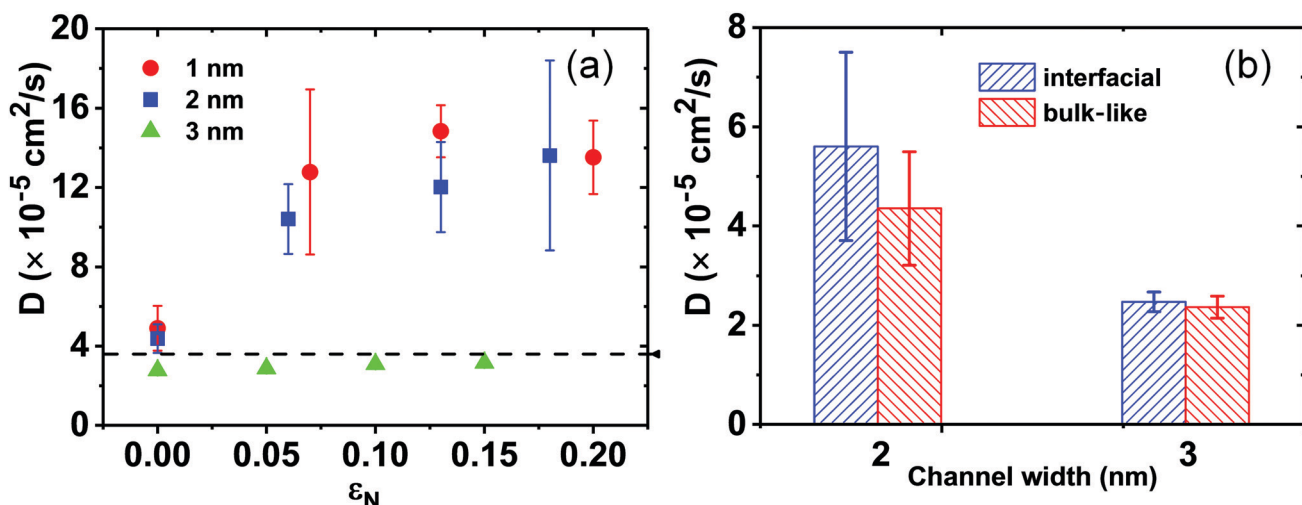
We also studied the impact of stretching coefficient on the hydrogen bond length and intermittent lifetime to further understand the dynamic properties of confined water. Two water molecules are considered to be hydrogen-bonded only if the hydrogen bond length is shorter than or equal to 3.5 Å, and the angle formed by the vector of the two oxygen atoms of water and one O-H vector is lower than 30°.<sup>47</sup> The hydrogen bond length distribution probability and the ACF of hydrogen bonds of stretched water within various graphene channels are displayed in Fig. 5. Fig. 5a–c show that the hydrogen bond length becomes slightly longer with the increase of stretching coefficient, due to the increased distance between water molecules. With the increase of the width of graphene channel, the impacts of stretching coefficient on hydrogen bond length distribution probability become less significant. In addition,

Fig. 5d–f show that the ACFs of confined water within the graphene channel decay slower than bulk water, implying an extended lifetime of the hydrogen bond for confined water, similar to the findings of Kumar *et al.*<sup>5</sup> and Hummer *et al.*<sup>48</sup> The hydrogen bond life time of bulk water reported in this work agrees well with a previous study.<sup>32</sup> Such a phenomenon may be attributed to stronger hydrogen bonding between confined water molecules.<sup>5</sup> With the increase of stretching coefficient, the hydrogen bond lifetime of confined water is shorter, as shown in the inset of Fig. 5d, in the channel with  $L = 1$  nm. This could be due to the increased bulk-like region in the large nanochannels. However, the hydrogen bond lifetime of confined water is slightly longer with the increase of channel width. Besides, the longer life of the hydrogen bond in the channel with  $L = 1$  nm than those of  $L = 2$  and 3 nm may be attributed to the narrow confinement that facilitates hydrogen bonding. Overall, the higher stretching coefficient results in the longer hydrogen bond lifetime with a reduced ACF decay rate.

In order to reveal the effects of stretching coefficient on the diffusion of confined water, the self-diffusion coefficients of confined water within various channels are shown in Fig. 6a. Compared with bulk water, the diffusion coefficient of confined water increased, which may be relevant to the decreased magnitudes of the dipoles of the water molecules in the interfacial regions, as reported in a previous study.<sup>35</sup> Martí *et al.*<sup>49</sup> also demonstrated that confined water exhibited higher diffusivity than bulk by MD simulations. Besides, with the increasing stretching coefficient, the diffusion was greatly enhanced by approximately five times especially for  $L = 1$  and 2 nm. Netz *et al.*<sup>50</sup>



**Fig. 5** The hydrogen bond length distribution probability and the autocorrelation function, along with its lifetime, of stretched water confined within various graphene channels at 300 K, respectively. The left, middle and right panels represent cases of (a and d)  $L = 1$  nm, (b and e)  $L = 2$  nm and (c and f)  $L = 3$  nm, respectively. Black dashed lines represent the results of bulk water. The insets of (d–f) indicates the hydrogen bond lifetime of water within the channels of (d)  $L = 1$  nm, (e) 2 nm and (f) 3 nm, respectively. Red dashed lines represent the diffusion coefficient of bulk water.



**Fig. 6** The self-diffusion coefficient ( $D$ ) of confined water in graphene nanochannels at 300 K. (a) The self-diffusion coefficient of all confined water under stretching within  $L = 1, 2$  and  $3$  nm. The black dashed line represents the self-diffusion coefficient of bulk water ( $3.6 \times 10^{-5} \text{ cm}^2 \text{ s}^{-1}$ ) computed through a system of 885 water molecules under identical ambient conditions. (b) Comparison of self-diffusion coefficient ( $D$ ) of confined water of the interfacial region (the first peak in the density distribution profile of Fig. 3b and c) and the bulk-like region at  $\varepsilon_N = 0$ . There is no bulk-like region for the case of  $L = 1$  nm.

reported that decreasing the density of bulk water (similar to stretching) resulted in an increased self-diffusion coefficient due to the enhanced tetrahedral ordering. A recent study of Jalalitalab *et al.*<sup>51</sup> reported that with the decrease of densities of water confined in a channel of  $L = 0.8$  nm, a significant increase in self-diffusion coefficient was observed from MD simulations. Jiao *et al.*<sup>52</sup> investigated the diffusion of water confined in a graphene channel of  $L = 0.65$  nm, in which the collective diffusion

coefficients of water increased from  $1.49 \times 10^{-5} \text{ cm}^2 \text{ s}^{-1}$  to  $30.87 \times 10^{-5} \text{ cm}^2 \text{ s}^{-1}$  when the number of water molecules decreased from 986 to 58. Such a tendency is driven by thermal fluctuation. Ma *et al.*<sup>53</sup> observed an exceedingly faster diffusion than bulk water by simulating a water nanodroplet on a graphene sheet, and the self-diffusion coefficient showed a remarkable increase with the reduced number of water molecules within the nanodroplet. Actually, either tuning the density or the number of

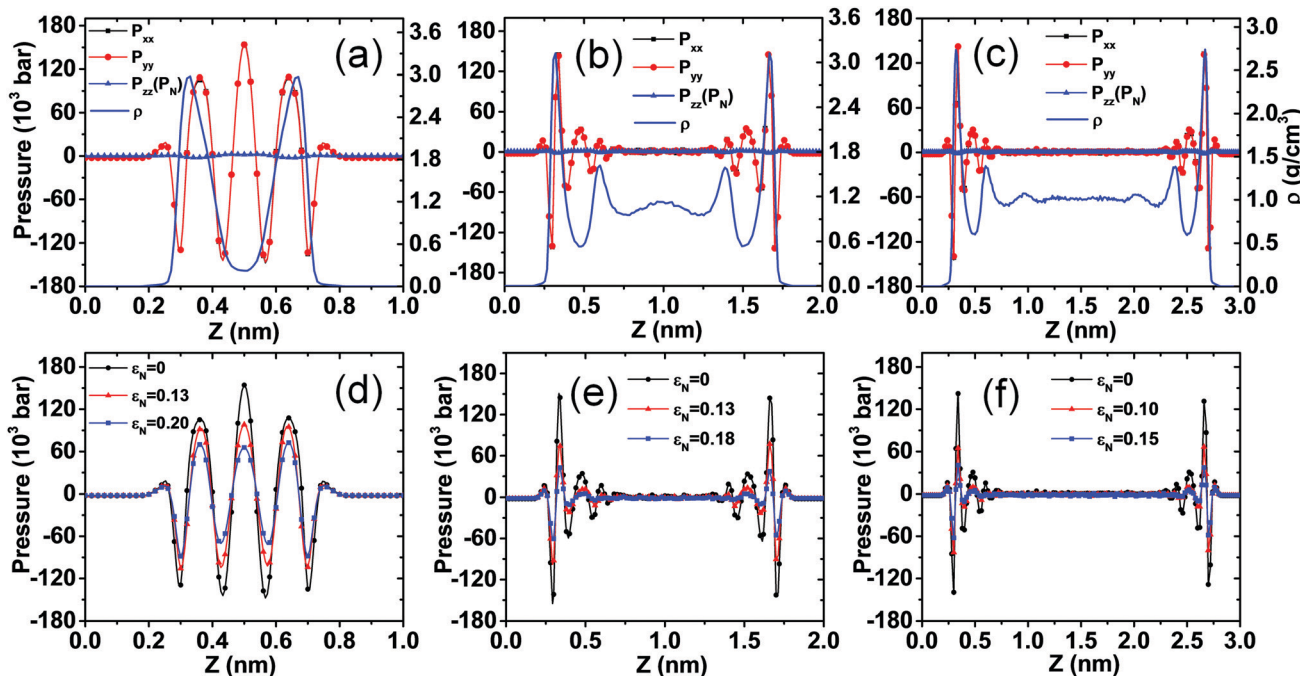


**Fig. 7** The total and dimensional pressure tensor profiles of water confined within various channel widths at varying stretching coefficients at 300 K. (a–c) Represent pressure tensors of three directions for (a)  $L = 1$  nm, (b)  $L = 2$  nm and (c)  $L = 3$  nm. The right-y axis describes the density profile along the  $z$  direction represented by blue solid lines. (e and f) Represent the tangential ( $P_T$ ) pressure tensor profiles under stretching at 300 K for (d)  $L = 1$  nm, (e)  $L = 2$  nm and (f)  $L = 3$  nm.

water molecules in confinement is equivalent to stretching water in confinement, leading to strong cohesive forces between confined water molecules (*i.e.*, the high negative pressure) that may facilitate the diffusion of water molecules. However, a decrease in self-diffusion coefficient of confined water compared with bulk water has also been reported,<sup>38,41,54</sup> which may be ascribed to the absence of stretching effects (by stretching and decreasing the density or number of water molecules in a simulation box) on diffusion. Thus, a higher density or more compacting water molecules than the bulk lead to the reduced diffusion coefficients. However, so far, the mechanism of the enhanced self-diffusion coefficient of stretched water within graphene nanochannels is still inconclusive, and it may depend on multiple factors including the channel properties, temperature and pressure.<sup>55,56</sup> Further comparison of the self-diffusion coefficient of water in the interfacial and bulk-like regions, respectively, revealed that the enhancement in  $D$  mainly resulted from the faster diffusion of the water in the interfacial regions, especially diffusion in the  $x$  and  $y$  directions (Fig. S2, ES<sup>†</sup>), which becomes insignificant with the increase of channel width (Fig. 6b). Therefore, water in  $L = 1$  nm exhibits the highest diffusion coefficient since it has no bulk region. Similar findings have been reported by Kumar *et al.*<sup>57</sup> and Rana *et al.*<sup>58</sup>

The anomalous high pressure of confined water has been reported by Gubbins' group.<sup>59,60</sup> In order to elucidate the impacts of stretching extent on internal pressure, we calculated the pressure tensors shown in Fig. 7 by Gromacs-LS,<sup>61,62</sup> including the tangential pressure along the  $x$  or  $y$  directions ( $P_{xx} = P_{yy}$  and  $P_T = (P_{xx} + P_{yy})/2$ , thus  $P_{xx} = P_{yy} = P_T$ ) and normal

pressure along the  $z$  direction ( $P_{zz} = P_N$ ). It was found that  $P_{xx}$ ,  $P_{yy}$  and  $P_T$  generally correlate with the density distribution profile inside graphene channels, suggesting that the confined water is composed of alternating layers exhibiting ultra-high positive and negative pressures regardless of the channel widths. In contrast,  $P_{zz}$  is nearly constant, similar to the studies of Vanegas *et al.*<sup>62</sup> and Long *et al.*<sup>30</sup> With the increase of channel width, the oscillating region is localized at the graphene–water interface. Moreover, the increased stretching coefficient weakens the oscillation and reduces the pressure values (Fig. 7d–f), facilitating the increased diffusion of water under stretching since either decreased positive pressure or negative pressure can result in the faster diffusion.

## 4. Conclusions

In this work, MD simulations have been performed to explore various structural and dynamic properties of the stretched water confined inside graphene channels with different widths (*i.e.*,  $L = 1$  nm, 2 nm and 3 nm) at 300 K. It was found that when the stretching coefficient increased, the density peak intensity decreased regardless of the channel width, and the location of the density peak slightly shifted towards the central region. Besides, the interfacial water molecules prefer to lie parallel to the graphene surface, facilitating the hydrogen bonding of confined water. Moreover, confined water within the graphene channel exhibits less tetrahedral ordering than bulk water with the increased stretching coefficient, which may be attributed to

the aggregation of water near graphene surfaces, leading to the breaking of the tetrahedral structure. Similarly, the long hydrogen bond length and the short lifetime of the hydrogen bond for confined water, compared with water, was observed, which decreased with the increase of stretching coefficient. The impacts of length and lifetime of the hydrogen bond of confined water will be weakened by the increasing channel width. On the other hand, the significantly increased self-diffusion coefficient of stretched water was demonstrated, especially inside small channels, which mainly resulted from the faster diffusion of water of interfacial regions. Both enhanced and reduced diffusion of confined water has been reported in previous studies by MD simulations, which can be possibly explained by the presence or absence of stretching effects through tuning the water density or number of water molecules within the confined space. The pressure distribution profiles of stretched water pressure demonstrated that confined water consists of multiple layers exhibiting ultra-high alternate positive and negative pressures (*i.e.*,  $P_{xx}$  and  $P_{yy}$ ) along graphene surfaces, and with the increased stretching coefficient, the oscillated  $P_{xx}$  and  $P_{yy}$  were reduced, corresponding to the enhanced diffusion along the channel surface. This work systematically investigated the effects of stretching extent on the structure and dynamic properties of confined water under varying channel widths, demonstrating the more disordered structure and increased diffusion of water under stretching, which may provide insights into understanding the molecular behavior of confined water under stretching.

## Conflicts of interest

There are no conflicts to declare.

## Acknowledgements

This work was supported by the National Natural Science Foundation of China (NSFC) under Project No. 51606081, 51606082 and double first-class research funding of China-EU Institute for Clean and Renewable Energy (No. ICARE-RP-2018-HYDRO-001). This work was carried out at National Supercomputer Center in Shenzhen.

## References

- D. Lucent, V. Vishal and V. S. Pande, *Proc. Natl. Acad. Sci. U. S. A.*, 2007, **104**, 10430.
- B. J. Berne, J. D. Weeks and R. Zhou, *Annu. Rev. Phys. Chem.*, 2009, **60**, 85–103.
- G. Xue, Y. Xu, T. Ding, J. Li, J. Yin, W. Fei, Y. Cao, J. Yu, L. Yuan, L. Gong, J. Chen, S. Deng, J. Zhou and W. Guo, *Nat. Nanotechnol.*, 2017, **12**, 317.
- M. Foroutan, S. M. Fatemi and F. Esmaelian, *Eur. Phys. J. E: Soft Matter Biol. Phys.*, 2017, **40**, 19.
- H. Kumar, C. Dasgupta and P. K. Maiti, *RSC Adv.*, 2015, **5**, 1893–1901.
- E. B. Moore, E. de la Llave, K. Welke, D. A. Scherlis and V. Molinero, *Phys. Chem. Chem. Phys.*, 2010, **12**, 4124–4134.
- R. H. Tunuguntla, R. Y. Henley, Y.-C. Yao, T. A. Pham, M. Wanunu and A. Noy, *Science*, 2017, **357**, 792.
- R. R. Nair, H. A. Wu, P. N. Jayaram, I. V. Grigorieva and A. K. Geim, *Science*, 2012, **335**, 442.
- G. Algara-Siller, O. Lehtinen, F. C. Wang, R. R. Nair, U. Kaiser, H. A. Wu, A. K. Geim and I. V. Grigorieva, *Nature*, 2015, **519**, 443.
- K. Koga, G. T. Gao, H. Tanaka and X. C. Zeng, *Phys. A*, 2002, **314**, 462–469.
- D. Ortiz-Young, H.-C. Chiu, S. Kim, K. Voitchovsky and E. Riedo, *Nat. Commun.*, 2013, **4**, 2482.
- J. C. T. Eijkel and A. V. D. Berg, *Microfluid. Nanofluid.*, 2005, **1**, 249–267.
- J. Gao, Y. Feng, W. Guo and L. Jiang, *Chem. Soc. Rev.*, 2017, **46**, 5400–5424.
- H. G. Park and Y. Jung, *Chem. Soc. Rev.*, 2014, **43**, 565–576.
- B. Radha, A. Esfandiar, F. C. Wang, A. P. Rooney, K. Gopinadhan, A. Keerthi, A. Mishchenko, A. Janardanan, P. Blake, L. Fumagalli, M. Lozada-Hidalgo, S. Garaj, S. J. Haigh, I. V. Grigorieva, H. A. Wu and A. K. Geim, *Nature*, 2016, **538**, 222.
- X. Song, L. Lu, M. Wei, Z. Dai and S. Wang, *Mol. Simul.*, 2018, **1**–10, DOI: 10.1080/08927022.2018.1510179.
- F. Caupin and A. D. Stroock, *Liquid Polymorphism, Book Series: Advances in Chemical Physics*, 2013, vol. 152, pp. 51–80.
- H. Cochard, *C. R. Phys.*, 2006, **7**, 1018–1026.
- P. F. Scholander, E. D. Bradstreet, E. A. Hemmingsen and H. T. Hammel, *Science*, 1965, **148**, 339.
- T. D. Wheeler and A. D. Stroock, *Nature*, 2008, **455**, 208.
- P. Wang, W. Gao, J. Wilkerson, K. M. Liechti and R. Huang, *Extreme Mech. Lett.*, 2017, **11**, 59–67.
- M. Nazari, A. Masoudi, P. Jafari, P. Irajizad, V. Kashyap and H. Ghasemi, *Langmuir*, 2019, **35**, 78–85.
- C. Duan, R. Karnik, M.-C. Lu and A. Majumdar, *Proc. Natl. Acad. Sci. U. S. A.*, 2012, **109**, 3688–3693.
- W. L. Jorgensen, J. Chandrasekhar, J. D. Madura, R. W. Impey and M. L. Klein, *J. Chem. Phys.*, 1983, **79**, 926–935.
- A. K. Rappe, C. J. Casewit, K. S. Colwell, W. A. Goddard and W. M. Skiff, *J. Am. Chem. Soc.*, 1992, **114**, 10024–10035.
- K. Liu, P. Yang, S. Li, J. Li, T. Ding, G. Xue, Q. Chen, G. Feng and J. Zhou, *Angew. Chem., Int. Ed.*, 2016, **55**, 8003–8007.
- D. Dubbeldam, S. Calero, D. E. Ellis and R. Q. Snurr, *Mol. Simul.*, 2016, **42**, 81–101.
- B. Hess, C. Kutzner, D. van der Spoel and E. Lindahl, *J. Chem. Theory Comput.*, 2008, **4**, 435–447.
- T. Darden, D. York and L. Pedersen, *J. Chem. Phys.*, 1993, **98**, 10089–10092.
- Y. Long, J. C. Palmer, B. Coasne, M. Śliwińska-Bartkowiak, G. Jackson, E. A. Müller and K. E. Gubbins, *J. Chem. Phys.*, 2013, **139**, 144701.
- N. C. Admal and E. B. Tadmor, *J. Elasticity*, 2010, **100**, 63–143.
- H. Xu, H. A. Stern and B. J. Berne, *J. Phys. Chem. B*, 2002, **106**, 2054–2060.

- 33 S.-P. Ju, C.-I. Chang, M.-H. Weng and N.-K. Hsieh, *J. Phys. Chem. C*, 2009, **113**, 7484–7491.
- 34 W. Gao, K. M. Liechti and R. Huang, *Extreme Mech. Lett.*, 2015, **3**, 130–140.
- 35 G. Cicero, J. C. Grossman, E. Schwegler, F. Gygi and G. Galli, *J. Am. Chem. Soc.*, 2008, **130**, 1871–1878.
- 36 L. Cheng, P. Fenter, K. L. Nagy, M. L. Schlegel and N. C. Sturchio, *Phys. Rev. Lett.*, 2001, **87**, 156103.
- 37 S. H. Lee and P. J. Rossky, *J. Chem. Phys.*, 1994, **100**, 3334–3345.
- 38 H. Mosaddeghi, S. Alavi, M. H. Kowsari and B. Najafi, *J. Chem. Phys.*, 2012, **137**, 184703.
- 39 J. Martí, J. Sala, E. Guàrdia and M. C. Gordillo, *Phys. Rev. E: Stat., Nonlinear, Soft Matter Phys.*, 2009, **79**, 031606.
- 40 M. C. Gordillo and J. Martí, *Phys. Rev. B: Condens. Matter Mater. Phys.*, 2008, **78**, 075432.
- 41 P. Hirunsit and P. B. Balbuena, *J. Phys. Chem. C*, 2007, **111**, 1709–1715.
- 42 J. R. Errington and P. G. Debenedetti, *Nature*, 2001, **409**, 318.
- 43 Y. I. Jhon, K. T. No and M. S. Jhon, *Fluid Phase Equilib.*, 2006, **244**, 160–166.
- 44 A. Stukowski, *JOM*, 2014, **66**, 399–407.
- 45 A. Stukowski, *Modell. Simul. Mater. Sci. Eng.*, 2009, **18**, 015012.
- 46 M.-Y. Zhao, X.-P. Yang and X.-N. Yang, *Acta Phys.-Chim. Sin.*, 2015, **31**, 1489–1498.
- 47 A. Luzar and D. Chandler, *J. Chem. Phys.*, 1993, **98**, 8160–8173.
- 48 G. Hummer, J. C. Rasaiah and J. P. Noworyta, *Nature*, 2001, **414**, 188.
- 49 J. Martí, J. Sala and E. Guàrdia, *J. Mol. Liq.*, 2010, **153**, 72–78.
- 50 P. A. Netz, F. W. Starr, H. E. Stanley and M. C. Barbosa, *J. Chem. Phys.*, 2001, **115**, 344–348.
- 51 E. Jalalitalab, M. Abbaspour and H. Akbarzadeh, *New J. Chem.*, 2018, **42**, 16258–16272.
- 52 S. Jiao and Z. Xu, *ACS Nano*, 2017, **11**, 11152–11161.
- 53 M. Ma, G. Tocci, A. Michaelides and G. Aepli, *Nat. Mater.*, 2015, **15**, 66.
- 54 Y. Liu, Q. Wang, T. Wu and L. Zhang, *J. Chem. Phys.*, 2005, **123**, 234701.
- 55 I. N. Tsimpanogiannis, O. A. Moulton, L. F. M. Franco, M. B. D. M. Spera, M. Erdős and I. G. Economou, *Mol. Simul.*, 2018, 1–29, DOI: 10.1080/08927022.2018.1511903.
- 56 M. Moulod and G. Hwang, *J. Appl. Phys.*, 2016, **120**, 194302.
- 57 P. Kumar, S. V. Buldyrev, F. W. Starr, N. Giovambattista and H. E. Stanley, *Phys. Rev. E: Stat., Nonlinear, Soft Matter Phys.*, 2005, **72**, 051503.
- 58 M. K. Rana and A. Chandra, *J. Chem. Phys.*, 2013, **138**, 204702.
- 59 Y. Long, M. Śliwińska-Bartkowiak, H. Drozdowski, M. Kempinski, K. A. Phillips, J. C. Palmer and K. E. Gubbins, *Colloids Surf. A*, 2013, **437**, 33–41.
- 60 M. Śliwińska-Bartkowiak, H. Drozdowski, M. Kempinski, M. Jaźdżewska, Y. Long, J. C. Palmer and K. E. Gubbins, *Phys. Chem. Chem. Phys.*, 2012, **14**, 7145.
- 61 A. Torres-Sánchez, J. M. Vanegas and M. Arroyo, *J. Mech. Phys. Solids*, 2016, **93**, 224–239.
- 62 J. M. Vanegas, A. Torres-Sánchez and M. Arroyo, *J. Chem. Theory Comput.*, 2014, **10**, 691–702.